CHEMISTRY
A EUROPEAN JOURNAL

DOI: 10.1002/chem.201003763

Conformationally Controlled Electron Delocalization in n-Type Rods: Synthesis, Structure, and Optical, Electrochemical, and Spectroelectrochemical Properties of Dicyanocyclophanes

David Vonlanthen,[a] Alexander Rudnev,[b, c] Artem Mishchenko,[b] Alexander Käslin,[a] Jürgen Rotzler,[a] Markus Neuburger,[a] Thomas Wandlowski,*[b] and Marcel Mayor*[a, d]

Abstract: A series of dicyanobiphenylcyclophanes **1–6** with various π-backbone conformations and characteristic n-type semiconductor properties is presented. Their synthesis, optical, structural, electrochemical, spectroelectrochemical, and packing properties are investigated. The X-ray crystal structures of all n-type rods allow the systematic correlation of structural features with physical properties. In addition, the results are supported by quantum mechanical calculations based on density functional theory. A two-step reduction process is observed for all n-type rods, in which the first step is reversible. The potential gap between the reduction processes depends linearly on the $\cos^2$ value of the torsion angle φ between the π-systems. Similarly, optical absorption spectroscopy shows that the vertical excitation energy of the conjugation band correlates with the $\cos^2$ value of the torsion angle φ. These correlations demonstrate that the fixed intramolecular torsion angle φ is the dominant factor determining the extent of electron delocalization in these model compounds, and that the angle φ measured in the solid-state structure is a good proxy for the molecular conformation in solution. Spectroelectrochemical investigations demonstrate that conformational rigidity is maintained even in the radical anion form. In particular, the absorption bands corresponding to the SOMO–LUMO+i transitions are shifted bathochromically, whereas the absorption bands corresponding to the HOMO–SOMO transition are shifted hypsochromically with increasing torsion angle φ.

Keywords: conjugation · cyanides · cyclophanes · electrochemistry · medium-ring compounds

Introduction

The potential of cheap solar cells, field-effect transistors, and organic light-emitting diodes (OLEDs) is fueling interest in organic semiconductor materials.[1]

The performance of such devices critically depends on the efficiency with which charge carriers (holes and electrons) move within π-conjugated materials. Organic semiconductors can be divided into two classes: p-channel semiconductors (holes are injected into the material from the electrodes), and n-channel semiconductors (electrons can be injected into the material from the electrodes). The availability of both efficient n- and p-channel semiconductor materials is one of the bottlenecks currently limiting the development of electronic devices.

For the development of efficient π-conjugated materials, a profound understanding of the interplay between the π-electron delocalization and geometrical structural features is required. The structure/property relationships of π-conjugated polymers[1a,2] or molecular rods[3] with p-type character have been studied extensively during the last few years. Most of these semiconductors are based on organic systems with electron-rich, oxidizable structures comprising thiophene,[2b] pyrrole, or other systems containing nitrogen donors.[2a] In contrast, the structure/property correlations of n-channel materials have not been well established because of the lim-

[a] Dr. D. Vonlanthen, A. Käslin, J. Rotzler, M. Neuburger, Prof. Dr. M. Mayor
Department of Chemistry, University of Basel
St. Johanns-Ring 19, 4056 Basel (Switzerland)
Fax: (+41) 61-267-10-06
E-mail: marcel.mayor@unibas.ch

[b] Dr. A. Rudnev, Dr. A. Mishchenko, Prof. Dr. T. Wandlowski
Department of Chemistry and Biochemistry
University of Bern Freiestrasse 3
3012 Bern (Switzerland)
Fax: (+41) 31-631-3994
E-mail: thomas.wandlowski@dcb.unibe.ch

[c] Dr. A. Rudnev
A.N. Frumkin Institute of Physical Chemistry and Electrochemistry,
Russian Academy of Sciences, Leninskii pr. 31
119991 Moscow (Russia)

[d] Prof. Dr. M. Mayor
Institute of Nanotechnology
Karlsruhe Institute of Technology (KIT)
P.O. BOX 3640, 76021, Karlsruhe (Germany)
Fax: (+49) 724-82-56-85
E-mail: marcel.mayor@kit.edu

Supporting information for this article is available on the WWW under http://dx.doi.org/10.1002/chem.201003763.

ited availability of stable and highly performing electron-accepting π-systems.[1a,4] Prototypical polymeric n-channel materials usually consist of rather rigid molecular subunits such as naphthalene or perylene tetracarboxylic diimides.[5] Progress in the development of new types of n-channel semiconductors has been made in the past few years through chemical substitution of the aromatic subunits with electron-withdrawing groups.[4b] Strong acceptor groups efficiently lower the frontier orbital levels, and thereby make the structure LUMOs accessible to electrons at less negative potentials. In other words, these acceptor groups can improve the reducibility of the system. However, a clear relationship between the spatial arrangement of neighboring π-systems and electronic properties is still lacking.

Recently, it has been shown that the conformation of individual subunits in polymeric chains such as poly(phenylene vinylene) is crucial in determining the overall physical properties of the material.[6] Furthermore, charge transport in biphenyl model structures comprising donor substituents has been studied, showing that electronic hole transport through the HOMO depends linearly on the $\cos^2$ value of the torsion angle between the two divided π-systems.[3]

The exploration of the extent to which these findings also apply to electrons delocalized in the LUMOs was the motivation for the physical investigations of the series of model compounds presented here.

Results and Discussion

Molecular design of dicyanocyclophanes as model compounds with tunable backbone conjugation: Six dicyanobiphenyls (**1**–**6**) were designed as a series of model compounds

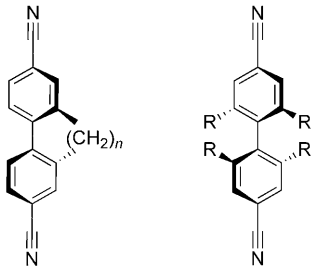

1: n = 1
2: n = 2
3: n = 3
4: n = 4

5: R = H
6: R = CH_3

with comparable lengths and substitution patterns, but with different torsion angles φ between the phenyl rings as the only varying structural feature.[3a] The torsion angle φ can be fixed by interconnecting the two benzonitrile units with a second short alkyl chain fixed in the 2 and 2′ positions. Thus, the number of CH_2 units dictates the torsion angle φ, and therefore the degree of π-electron delocalization between the two π-systems, while the overall electronic structure is maintained. Furthermore, the steric requirements of the chemically inert alkyl substituents potentially prevent intermolecular aggregation.

Substitution of the terminal positions of the biphenyl synthons with cyano groups improves the ease of electron injection into the π-system. As a consequence, the reduction potential of the benzonitrile subunit becomes electrochemically accessible, and thus becomes a label for the investigation of the inter-ring communication.

Furthermore, with the terminal cyano groups as potential anchor groups for metal electrodes, this series of model compounds is ideally suited for studying electron transport on a single-molecule level. Thereby, the series enables the systematic investigation of the relationship between electron transport and backbone conformation, which is reported elsewhere.[7]

In addition, organic cyano derivates are highly stable compounds compared to thiols,[8] amines,[9] or isocyanides.[10]

In the following, we present the synthesis of six model compounds (**1**–**6**) with n-channel semiconductor properties. Subsequently, we describe and discuss their solid-state molecular structures and packing properties, and correlate these data with their electrochemical, spectroelectrochemical, and optical characteristics. Moreover, single crystals of all members of the series were grown, revealing information about the molecular structures and packing properties in the solid state. The experimental data are compared with results obtained from DFT calculations.

Synthesis of the dicyanocyclophanes: The synthetic strategy for building the cyclophane synthons was based on our previously reported work on angle-restricted biphenyldithiols.[3a,11a]

Cyclophanes **1**–**4**, with increasing inter-ring alkyl chain length (n = 1–4) and thus with increasing torsion angles, were our initial synthetic target structures. The series of terminally cyano-functionalized biphenyl systems was complemented by the unsubstituted compound **5**, and the 2,2′,6,6′-tetramethyl derivate **6**.

Within these terminally cyano-functionalized biphenyl systems, variations of the inter-ring torsion angles between 0° for the fluorene compound **1** and 90° for the tetramethylbiphenyl compound **6** were expected.

Here, we present an alternative synthetic route based on our recently published concept.[3a,11a] The strategy to build up the cyclophane structures **3** and **4** is adopted, but the terminal halogen atoms are replaced by methoxy groups. The new synthetic pathway can easily be scaled up to a few hundred grams, and no longer requires the use of polymethylhydrosiloxane, which is difficult to handle, and other costly reagents. Furthermore, the overall yield of this new "methoxy" synthetic route is increased almost four times compared to the previously described synthesis.[11a] The synthetic pathway of dicyanocyclophane **3** is shown in Scheme 1.

Starting from the bulk chemical 4-bromo-3-methylanisole, an oxidative iron-catalyzed homocoupling reaction,[12] using

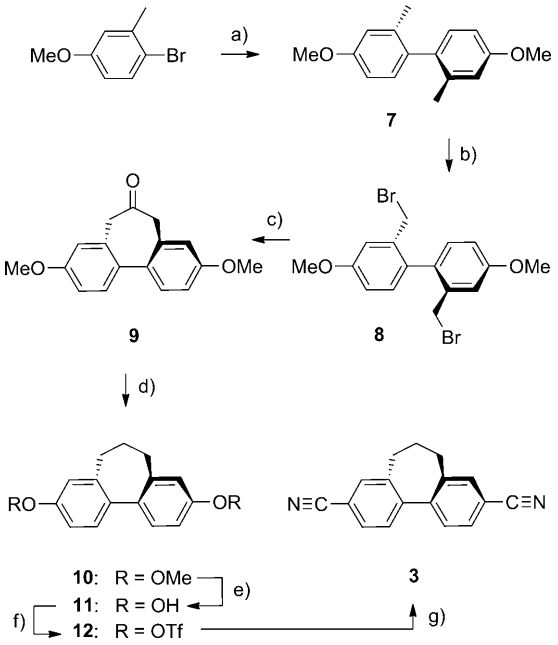

Scheme 1. Synthesis of the dicyanobiphenylcyclophane **3**. Reagents and conditions: a) Mg^0 (1.4 equiv), methyl-THF, $FeCl_3$ (7.1 mol%), 1,2-dichloroethane (1.7 equiv), reflux, 92%; b) NBS (2.1 equiv), benzoyl peroxide (7.5 mol%), CCl_4, reflux, 68%; c) TosMic (1.0 equiv), CH_2Cl_2, NaOH, tetrabutylammonium bromide (TBAB) (6.3 mol%), then HCl, *t*BME/H_2O, 83%; d) KOH (4.2 equiv), hydrazine monohydrate (2.3 equiv), diethylene glycol, 195°C, 86%; e) BBr_3 (5.5 equiv), CH_2Cl_2, 0°C to RT; f) Tf_2O (3.9 equiv), pyridine, RT, 84% over two steps; g) Method A: $[Pd_2(dba)_3]\cdot CHCl_3$ (10.0 mol%), xantphos (10.0 mol%), tributyltin chloride (3.6 mol%), KCN (3.0 equiv), acetonitrile, reflux, 82%.

stoichiometric amounts of 1,2-dichloroethane as the re-oxidation agent, afforded the building block **7** in 92% yield. Subsequent double bromination with *N*-bromosuccinimide (NBS) afforded the key intermediate **8** in 68% yield. To achieve the oxo-functionalized propyl bridge in **9**, an additional carbon atom was introduced through an intramolecular cyclization reaction of the dibromide **8**, using the masked formaldehyde equivalent (tolylsulfonyl)methyl isocyanide (TosMic)[13] to provide the dimethoxy ketone **9** as a white solid in a yield of 83%. The "methoxy" route allowed reduction through a Wolff–Kishner reaction,[14] affording **10** in 86% yield. This was considerably more efficient in terms of the purification procedure than the previously reported reduction protocol.[3a,11a]

Subsequent functional-group transformations allowed **10** (with terminal methoxy groups) to be transformed into **12** (bearing triflate groups).[11b] The unfunctionalized propyl bridge in **10** allowed electrophilic cleavage of the two methyl groups of the biaryl diether with boron tribromide at room temperature. Subsequent esterification of the diol **11** with triflic anhydride in pyridine gave the triflate building block **12** in a yield of 84% over two steps. An overall yield of 38% was obtained for this six-step reaction sequence.

The conversion of triflates to aryl nitriles is a valuable synthetic reaction because of the wide range of available environmentally friendly phenol derivatives. However, only a few examples of the conversion of triflate groups have been reported.[15] To the best of our knowledge, the synthesis of bis(triflate)-functionalized aromatic systems has not yet been investigated. The use of catalytic amounts of $[Pd_2(dba)_3]$, tributyltin chloride, and xantphos in refluxing acetonitrile (denoted as method A) was successful in the double cross-coupling reaction of **12** with potassium cyanide to give the model compound dicyanocyclophane **3** in 82% yield as white solid.

Again, starting from the key intermediate **8** (Scheme 2), a copper-mediated alkylation, with the Normant reagent generated in situ, provided the diallylbiphenyl **13** as a smelly oil

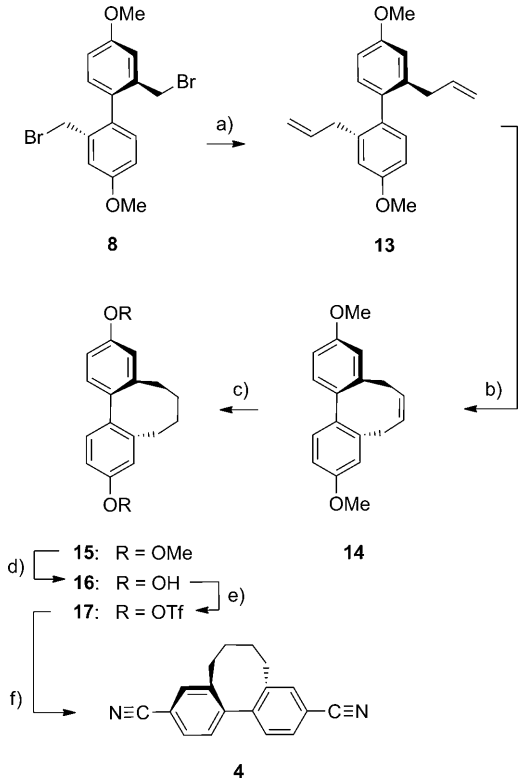

Scheme 2. Synthesis of the dicyanobiphenylcyclophane **4**. Reagents and conditions: a) $CH_2CHMgBr$ (6.0 equiv), CuI (1.0 equiv), CH_2Cl_2, −50°C to RT, 77%; b) Grubb's catalyst (5.0 mol%), CH_2Cl_2, reflux, 79%; c) H_2, Pd/C 10%, RT, EtOAc, 98%; d) BBr_3, pyridine, RT; e) Tf_2O (3.9 equiv), pyridine, RT, 83% over two steps; f) Method A: 86%.

in 77% yield. A ring-closing metathesis using Grubbs' catalyst afforded **14** in high yield (79%). Subsequent hydrogenation with Pd/C at atmospheric pressure gave the hydrogenated butyl-bridged biaryl ether **15** in almost quantitative yield. Finally, a similar deprotection/reprotection reaction sequence, as described for the synthesis of **12**, resulted in the transformation of the methoxy groups into triflate groups to provide the butyl-bridged key intermediate **17** in 83% yield over two steps (Scheme 2). An overall yield of 31% was obtained for this seven-step reaction sequence. Applying again

the cyanation method A to the ditriflate **17** afforded the model compound dicyanocyclophane **4** as a white solid in 86% yield after purification by flash chromatography.

Single crystals of model compounds **3** and **4** suitable for X-ray structural analysis were obtained by recrystallization from a mixture of hot dioxane and cyclohexane.

Whereas the model compounds **3** and **4** were assembled by the "methoxy route", another strategy was applied for the assembly of the dicyanocyclophanes **1** and **2**. Starting from 2,7-dibromofluorene,[16] a Rosenmund–Von Braun[17] reaction using copper(I) cyanide was performed (denoted as method B), yielding the fully planar dicyano compound **1** in 51% yield.

Although other authors[18] have already reported the synthesis of 2,7′-dicyanofluorene, a complete analytical characterization is still lacking. Repeated attempts to purify **1** were complicated because of the low solubility of the fluorene derivate. These attempts included repeated extraction of the product by ethyl acetate, and filtration through silica, followed by repeated recrystallization from 1) acetonitrile, 2) ethanol, and 3) 2-methoxyethanol, yielding crystalline samples of insufficient purity. A final chromatographic purification of **1** was achieved by dissolving the compound in a large amount of chloroform and adsorbing it to the immobilized phase. This was followed by recrystallization from a hot mixture of dioxane and cyclohexane, affording single crystals suitable for X-ray analysis as the first sample satisfying all analytical criteria.

The dicyanocyclophane **2** containing an ethylene bridge was assembled using a similar synthetic strategy. 2,7-Dibromo-9,10-dihydrophenanthrene[19] (**19**) underwent a cyanation reaction with copper(I) cyanide (method B), followed by recrystallization from hot toluene and subsequently from a boiling mixture of dioxane and cyclohexane, to give single crystals of **2** suitable for X-ray analysis (Scheme 3).

The model compound 4,4′-dicyanobiphenyl **5** was synthesized starting from the commercially available 4,4′-dibromobiphenyl **20**. Again, a doubly copper-mediated cyanation reaction (method B) afforded the target compound **5** in a yield of 73%. Due to the low solubility of the core-unsubstituted biphenyl **5**, similar purification problems were encountered as described before for the fluorene model compound **1**. An adapted purification procedure allowed the separation of the impurities of biphenyl **5**. The slow evaporation technique with dioxane/cyclohexane as the solvent mixture was a crucial step in obtaining single crystals suitable for X-ray analysis.

To complement the series of cyclophanes with restricted rotation along the biphenyl axis, we focused further on a biphenyl system with sterically demanding alkyl substituents at the positions *ortho* to the biphenyl bridge. The already available building block[11a,19] **21** with four methyl groups in the *ortho* positions was successfully cyanated by applying method B; the reaction was completed within a shorter reaction time and proceeded at a slightly lower reaction temperature. Purification by flash chromatography on silica followed by recrystallization from cyclohexane using the slow

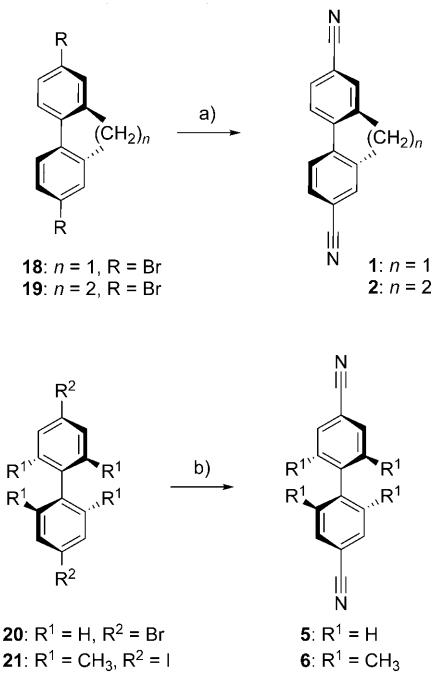

Scheme 3. Synthesis of the dicyanobiphenyl derivatives **1**, **2**, **5**, and **6**. Reagents and conditions: Method B: a) $Cu^{I}CN$ (2.6 equiv), DMF, 150–160°C, 51% for **1** and 53% for **2**; b) $Cu^{I}CN$ (3.0 equiv), DMF, 150–160°C, 16 h, 73% for **5**, and $Cu^{I}CN$ (3.0 equiv), DMF, 140°C, 8 h, 84% for **6**.

evaporation technique afforded the last member of the series **6** as single crystals.

All synthesized molecules were fully characterized by ^{1}H and ^{13}C NMR spectroscopy, mass spectrometry, optical absorption spectroscopy, and elemental analysis. Accurate mass determination was used instead of elemental analysis for some of the intermediates. In addition, all target structures **1–6** were analyzed using cyclic voltammetry, and their solid state structures were determined by X-ray analysis.

Solid-state structure analysis: X-ray solid state structure analysis of the new biphenyl model compounds **1–6** was of particular interest. Single crystals of the entire series were grown, not only to confirm the identity of the molecules and to provide highly pure model compounds, but also to investigate the correlation between the length of the bridging alkyl chain or the bulkiness of the substituents in the 2,2′,6,6′-positions in **1–6** and the resulting torsion angles φ.

Figure 1 displays the solid-state structures of the dicyano-derivates **1–6** as a series with increasing torsion angle. Furthermore, selected structural parameters such as the intramolecular nitrogen–nitrogen distance as the length axis of the molecule or the torsion angle φ are listed in Table 1, and are compared with the torsion angles obtained from the DFT calculations.

The torsion angles were measured between the planes of the phenyl rings of the biphenyl skeleton. These planes were obtained by considering all six carbon-atom positions of the

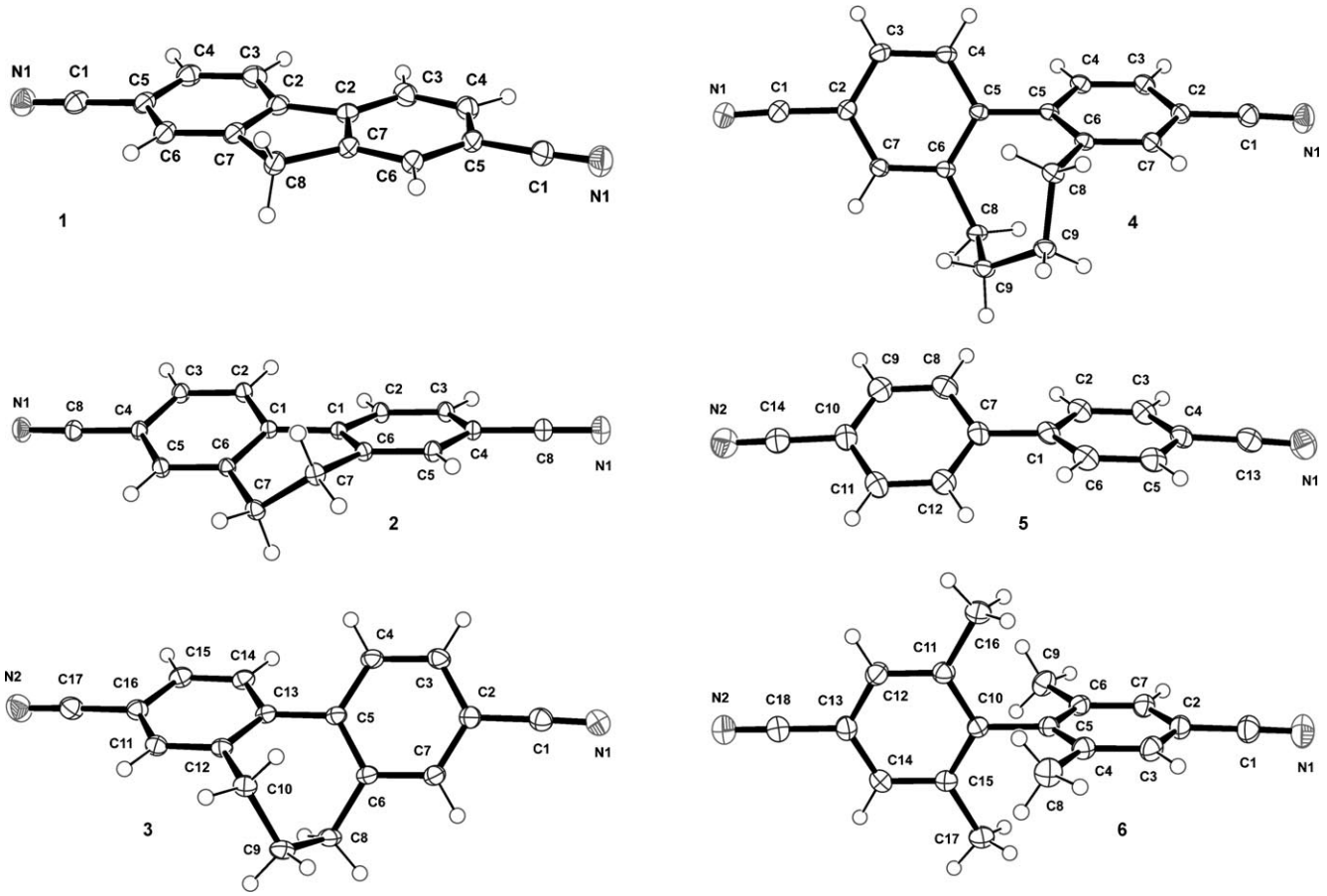

Figure 1. Solid-state structures of the dicyanobiphenyl derivatives **1–6**. Thermal ellipsoids are set at the 50% probability level.

Table 1. Molecular structures and measured properties.

	φ [°] solid state	φ [°] DFT[a]	N–N distance [Å]	crystal system	space group
1	1.02	0.00	11.96(9)	monoclinic	$P2/n$
2	20.74	20.97	12.22(3)	monoclinic	$C2/c$
3	44.78	47.13	12.24(5)	triclinic	$P\bar{1}$
4	58.47	59.94	12.24(6)	monoclinic	$C2/c$
5	31.77	39.60	12.20(2)	monoclinic	$P2_1$
6	89.26	90.00	12.21(4)	monoclinic	$P2_1/c$

[a] See next section for computational details.

solid-state structure for the least-squares minimization procedure. Very comparable intramolecular nitrogen–nitrogen distances were obtained within the series of X-ray-analyzed derivatives, with values between 11.96(9) Å for **1** and 12.24(6) Å for **4**. This indicates that the effects of the various alkyl substituents on the length of the dicyanocyclophane backbone are minimal.

As expected, a fully planar biphenyl backbone is observed in the fluorene structure **1**. Due to the bent backbone of **1**, the N–N distance of 11.96(9) Å is slightly decreased compared to all other derivatives. A continuous increase of the torsion angle is observed in the cyclophane structures **2–4** with elongation of the ring-interlinking alkyl chain. As shown in Table 1, all measured torsion angles are in good agreement with the values obtained from DFT calculations (see Table 1 and the next section for the calculations). Interestingly, the torsion angles of the dicyanocyclophane compounds **1–6** are very similar to those determined in an analogous series comprising terminal acetylsulfanyl donor substituents,[3a] indicating that the interlinking alkyl chain is the subunit dictating this structural feature of the biphenyl backbone. The core-unsubstituted biphenyl compound **5** is an exception. The torsion angle in the solid state was found to deviate from the value calculated theoretically in the gas phase by 7.83°. However, the torsion angle of unsubstituted biphenyl is reported to be strongly dependent on the state of aggregation and the temperature.[20]

An almost perpendicular arrangement of the two phenyl rings was measured for the solid-state structures of the tetramethyl model compound **6**, with a torsion angle φ of 89.26°. The rotation barriers of the methyl-substituted[21] model compound **6**, and in particular of the cyclophanes[22] **1–4**, are expected to increase considerably compared to the cyano-substituted derivative **5**, which is substituted solely in the *para* position.[23] Thus, the φ values measured in the solid state are considered to be a good proxy for the torsion angle expected in solution.

Of further interest was the packing motif of the model compounds **1–6** in the solid state. In Figure 2, the packing

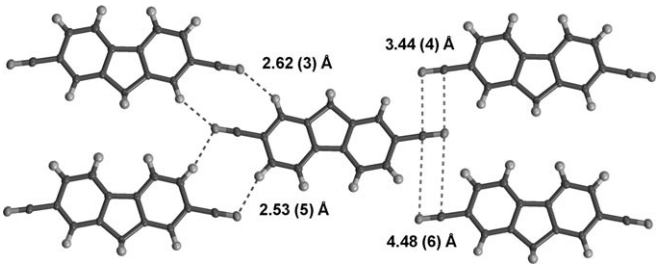

Figure 2. 1D chains of **1** in the solid-state structure stabilized by intermolecular contacts. The dipolar antiparallel CN···CN interactions are displayed on the right, and the weak hydrogen bond H_{Ar}···NC contacts are displayed on the left.

motif of the planar model compound **1** is shown as a representative example for the entire series of dicyanocyclophanes.

Figure 2 shows the top view of the molecular network. The molecules form 1D chains held together by dipolar antiparallel CN···CN interactions. Recently, experimental evidence for such dipolar CN···CN interactions has been systematically explored[24] by analyzing the Cambridge Structural Database. Furthermore, there are short H_{Ar}···NC contacts, in which the H···N distance is below 2.8 Å. These contacts can be interpreted as weak hydrogen bonds[25] (other similar contacts are omitted for clarity).

In addition, the packing structure is stabilized by the cofacial arrangement with the neighboring biphenyl planes.

The side view along the *b*-axis of the unit cell is displayed in Figure 3. Half of the fluorene molecule overlaps with the lower-lying and upper-lying molecules in a parallel displaced

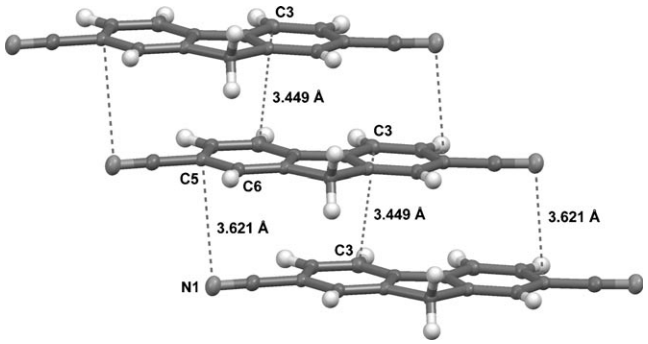

Figure 3. View along *b*-axis of the unit cell of the solid-state structure of **1** to display the cofacial through-space interactions.

manner, forming columnar π-stacks. The closest plane-to-plane distance between the two neighboring planar 2,7-dicyanofluorene units is found to be 3.44(9) Å between C3 and C3 of the parallel displaced rings. An additional stabilizing interaction may arise from the slightly positively polarized carbon atoms of the sp-hybridized cyano groups, which are sandwiched between the phenyl ring π-systems of the neighboring molecules supporting the intermolecular π–π stacking.

Comparable packing motifs with dipolar antiparallel CN···CN interactions and H_{Ar}···NC hydrogen bonds were observed in the packing structures of model compounds **2–6**. Generally, it is found that the intermolecular distances of these aggregates, stabilized by weak interactions, gradually increase with the increasing steric requirements of the alkyl chains and substituents attached to the phenyl rings. In particular, the increasing length of the ring-interlinking alkyl chain and attached methyl groups in the *ortho* position of the biphenyl bridge gradually enlarges the intermolecular distance between the cofacially arranged phenyl planes. The absence of efficient π–π overlap of the phenyl planes is observed if the interplanar torsion angle exceeds the value of 44.78°. Only dicyanocyclophane **1** (1.02°), **2** (20.74°), and the unsubstituted **5** (31.77°) display intermolecular distances between the planes of below 3.8 Å.[26]

Whereas weak intermolecular interactions play an important role in the overall stabilization of the packing structures of **1–6** in the solid state, intermolecular π–π aggregation of **1** was not observed in $CDCl_3$ and C_6D_6 in concentration-dependent NMR experiments.

Computational studies: In order to explore the geometries of the dicyanobiphenyls **1–6**, in particular with respect to their conformation and molecular orbital energies, ab initio calculations of the molecules in vacuum were performed. The geometry of each molecule was optimized using the TURBOMOLE program package[27] version 5.9, and DFT calculations with the B3LYP hybrid exchange correlation functional[28] in combination with the multiple accelerated resolution of identity in J (MARI-J) approximation[29] and the TZVP basis[30] set, as implemented in the TURBOMOLE program package.

In addition, the energy levels of the relaxed ground states of all structures in the series were calculated by DFT. All the calculated torsion angles and HOMO–LUMO energies are given in Table 2.

Table 2. Calculated torsion angles and energies of the dicyanocyclophane series.

	φ [°] DFT[a]	HOMO [eV]	LUMO [eV]	HOMO–LUMO separation [eV]
1	0.00	−6.94	−2.57	4.37
2	20.99	−6.92	−2.59	4.33
3	47.13	−7.09	−2.38	4.71
4	59.97	−7.14	−2.19	4.95
5	39.60	−7.21	−2.54	4.67
6	90.00	−7.39	−1.80	5.59

Whereas the twisted form of the simple biphenyl comprising various substituents in the *para* position is reported to be the dominant conformation in the gas phase and in solution,[31] planarization of the two phenyl rings occurs if, for example, molecule/surface[32] interactions dominate the weak steric repulsion[23] between the phenyl ring hydrogen atoms. In our calculations, the torsion angle of **5** turned out

to be relatively sensitive to the basis set used. The TZVP basis set gave a torsion angle of almost 40°, but calculations using the smaller basis set SVP gave a slightly reduced torsion angle of 36.96°. Incorporation of an alkyl chain of variable length in the 2,2′-position of the biphenyl skeleton controls the torsion angle between the two aromatic rings without changing the electronic environment of the π-system. As a result, the degree of electron π-delocalization is the only effect shifting the relative positions of the HOMO and LUMO levels. The LUMO level is stabilized, whereas the HOMO is destabilized with decreasing torsion angle. As a consequence, the energy gap increases with increasing torsion angle (Figure 4).

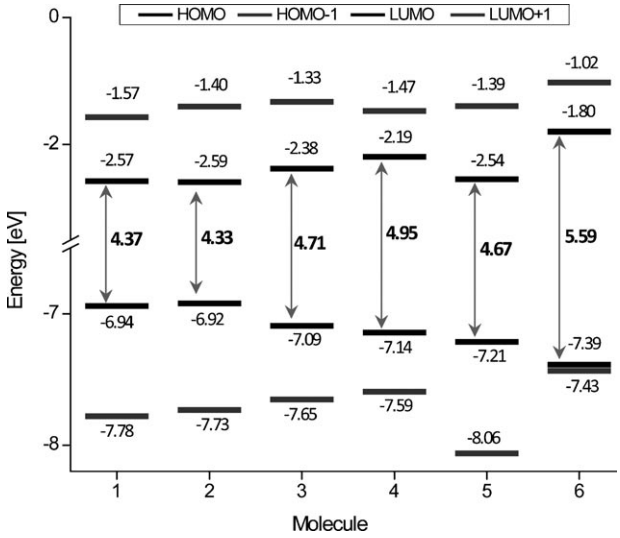

Figure 4. Energy diagram of the dicyanobiphenyl derivatives **1–6**. The energies are given in eV.

Compared to similar thiol-functionalized π-systems, the energy levels of the frontier orbitals of cyano-functionalized π-systems are downshifted in energy by ≈1.5 eV.[3b,33] The n-type semiconductor properties of cyano-functionalized π-systems are explained in particular by their lowered LUMO promoting efficient electron transport.[34]

The energy levels of the HOMO, LUMO, and their vicinal orbitals are visualized in Figure 4. Whereas DFT hybrid methods often underestimate ionization potentials and electron affinities, the HOMO–LUMO separations obtained with the B3LYP functional are reported to agree well with the vertical excitation energy of the UV absorption spectra.[35] Surprisingly, the calculation displays a slightly increased HOMO–LUMO separation for the fluorene structure **1** compared to the cyclophane structure **2**, which is no longer planar.

Electronic spectra: To investigate the correlation between the electronic properties and the interplanar torsion angle φ of the dicyanobiphenyls **1–6**, the absorption spectra of the entire series (1×10^{-5} M solutions) were recorded in acetonitrile (CH_3CN). All the recorded spectra are displayed in Figure 5, and a list of the most important UV absorption bands is given in Table 3.

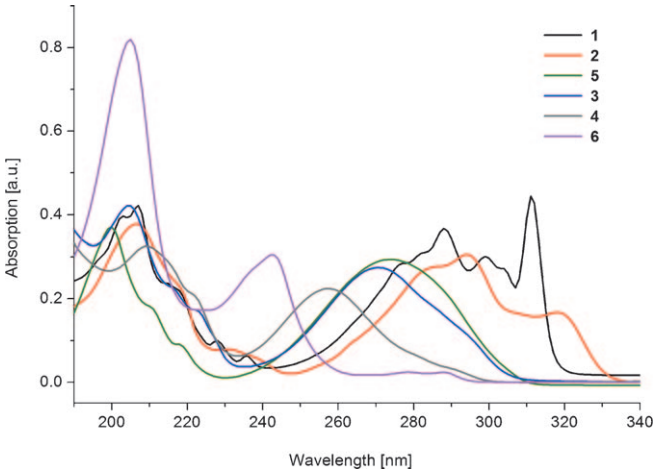

Figure 5. The overlaid UV absorption spectra of the dicyanocyclophane series **1–6** as 1×10^{-5} M solutions in CH_3CN.

Table 3. UV absorption properties of **1–6** in CH_3CN at 298 K.

	φ[a] [°]	λ_{max}[b] [nm (eV)]	ε[c] [L mol^{-1} cm^{-1}]	λ_{on}[d] [nm (eV)]
1	1.02	207 (5.99)	38600	322 (3.85)
		288 (4.31)	33500	
		299 (4.15)	27600	
		311 (3.99)	40800	
2	20.74	207 (5.99)	37800	335 (3.70)
		294 (4.22)	30600	
		318 (3.90)	16800	
3	44.78	204 (6.08)	42100	307 (4.04)
		271 (4.58)	27400	
4	58.47	209 (5.93)	32600	298 (4.16)
		257 (4.82)	22400	
5	31.77	199 (6.23)	60200	310 (4.00)
		274 (4.52)	38100	
6	89.26	205 (6.05)	81900	294 (4.22)
		243 (5.10)	30500	

[a] φ is the torsion angle between the planes of the phenyl rings as obtained from the solid-state structural analysis. [b] λ_{max} is the wavelength at the maximum of each band. [c] ε is the extinction coefficient at λ_{max} of each band. [d] λ_{on} is the onset of the absorption onset in the UV spectra.

The longest wavelength absorption band of **1** is at 311 nm, and, in analogy to its terminally unsubstituted counterparts, is, according to Clar,[36g] assigned to the α-absorption band (α-band, λ_{max} 300 nm).[36] Similarly, the structured absorption band between 275 and 293 nm can probably be assigned to the p-band of the biphenyl subunit, which exhibits a maximum absorption at 288 nm. The p-band of **1** displays a vibrational fine structure, presumably because of its rigid, essentially planar geometry. The bathochromic shift of the absorption bands compared to fluorene can be attributed to an enlargement of the π-system arising from the substitution with two cyano groups.[36d] The UV absorption spectra of compounds **1–6** were measured in acetonitrile, but negligible

solvatochromic effects were observed when using heptane as the solvent. Solvent effects investigated using molecular dynamics (MD) simulations of similar biphenyls showed negligible influence on the geometric structures.[7]

Cyano groups lead to an overall stabilization of the HOMO and LUMO levels,[37] as expected from the acceptor nature of the substituent. The p-band is also called the conjugation band (π–π* band),[36f,38] as its position is reported to reflect the extent of conjugation in the biphenyl core.[36f,38,39] The calculated HOMO/LUMO gaps of the series agree well with the vertical excitation energies of the p-band absorption,[35] and do not deviate by more than 0.15 eV for compounds **1**–**5** and 0.49 eV for compound **6**.

Surprisingly, for the terminally cyano-functionalized cyclophane **2**, which is no longer planar, we observe a bathochromic shift of 6–7 nm of both the p- (294 nm) and α- (318 nm) absorption bands with respect to the fluorene derivative **1**. Obviously, **2** exhibits the smallest optical band gap as well as the lowest vertical excitation energy within the series, which is consistent with the results obtained theoretically. In contrast to the terminally unsubstituted dihydrophenanthrene[38] (α-band, λ_{max} 298 nm), the longest wavelength absorption of cyclophane **2** shows a bathochromic shift of 20 nm. The onset of each absorption spectrum and all λ_{max} values are listed in Table 3. According to theory, the π–π* transition energy[36d,f] observable as the λ_{max} value of the conjugation band should correlate with the conformation of the biphenyl core. The orbital overlap of adjacent π-systems correlates linearly with $\cos\varphi$ between their planes, and the electron-transfer properties between the two π-systems are proportional to the $\cos^2$ values of their torsion angles.[40]

In Figure 6, the vertical π–π* excitation energy (p-band absorption maximum) of each compound under investigation is plotted against $\cos^2\varphi$. Within this series of compounds, the expected linear correlation between the vertical excitation energy and $\cos^2\varphi$ was observed.

The only exceptional behavior in the series was observed for the fluorene derivative **1**, which displays a vertical excitation energy outside this linear fit. However, the assignment of the structured UV bands of **1** is speculative. Results from first-principle calculations of the singlet excited states using TD-DFT and coupled cluster methods did not match the experimental results. DFT calculations of the ground state revealed a slightly larger HOMO–LUMO gap for **1** than for cyclophane **2**, which is no longer planar.

Whereas the interplanar torsion angles φ of all structures of this series were determined by solid-state structural analysis, that of the unsubstituted dicyanobiphenyl **5** (39.60°) was taken from the DFT calculations. In this particular case, the X-ray torsion angle is assumed to be dominated by packing effects, and therefore the calculated angle represents a more realistic situation in solution.[3b,41]

It is worth noting that the best-resolved spectrum was obtained for compound **1**. The broad band located at 250–340 nm has a set of sharp features for **1**, unlike that for the other compounds studied. 2,7-Dicyanofluorene represents a rather hard (rigid) structure, and prevents any changes in the conformation of this molecule, whereas molecules of the other compounds have a certain degree of freedom that results in the broadening of their absorption bands.

Electrochemistry: For the characterization of the electrochemical properties of the dicyanobiphenyls **1**–**6**, cyclic voltammograms (CVs) were recorded using a Au net electrode in a three-electrode all-glass electrochemical cell. 1,4-Dicyanobenzene (DCB) consisting of only one benzene ring was also investigated for comparison. Two pairs of reduction and oxidation peaks were observed for all the molecules studied (Figure 7).

The second (that is, more negative) reduction wave of **6** could not be resolved because of electrolyte decomposition

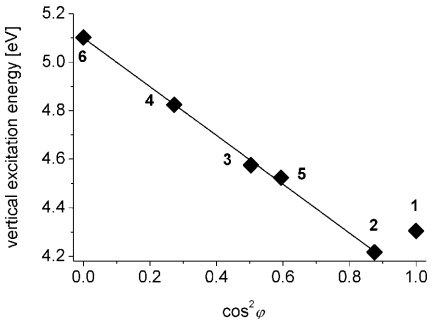

Figure 6. Vertical excitation energy for the lowest valence π–π* transition (p-band absorption maxima) of molecules **1**–**6** plotted against $\cos^2\varphi$ (φ is the interplanar torsion angle obtained from the X-ray structures). The torsion value of **5** was obtained from DFT calculations. The linear correlation coefficient R^2 (excluding **1**) is 0.9975.

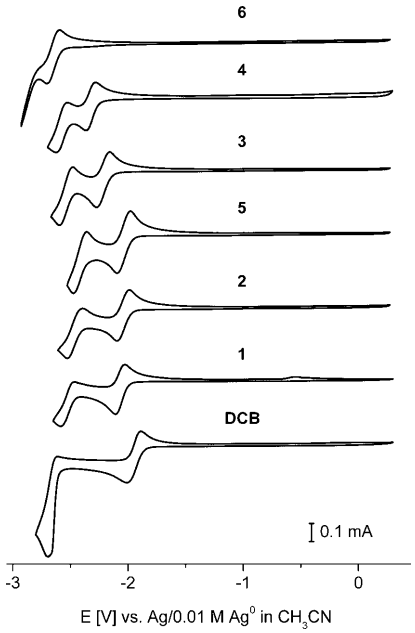

Figure 7. Cyclic voltammograms of the dicyanobiphenyl compounds **1**–**6** recorded from 0.5 mM solutions in a 0.1 M TBA·PF_6/CH_3CN electrolyte solution (scan rate 100 mV s^{-1}).

when employing a gold working electrode. However, both reduction waves of **6** were observed when using a glassy carbon electrode (GC, Figure S1 in the Supporting Information). We note that the redox potentials of the six dicyanobiphenyls **1**–**6** are, within $\Delta E_{red} < 10$ mV, identical on both Au and GC electrodes under the experimental conditions chosen. Calibration experiments with ferrocene revealed that both redox peaks represent one-electron processes.

Experiments with different scan rates (v) demonstrated that the peak-to-peak separation for each pair of redox peaks is larger than 59 mV, the expected value for an ideally reversible one-electron transfer process (Figure S2 in the Supporting Information). The difference increases with scan rate, with the reduction peaks (negative currents) showing a stronger shift than the corresponding oxidation peaks (positive currents) for both redox couples (Figure S3 in the Supporting Information). Furthermore, the peak heights increase linearly with the square root of scan rate, indicating a substantial contribution due to reactant diffusion (Figure S4 in the Supporting Information). The ratios between the reduction and oxidation currents of the first pair of peaks is close to one, whereas the second pair of peaks results in substantially smaller values. These observations clearly show that both redox processes correspond to quasi-reversible one-electron transfer reactions, with the more negative process most probably coupled to a follow-up reaction involving the partial decomposition of the reactant.[42]

On the basis of previous literature data,[43] we suggest that the first reduction wave represents the formation of the anion radical [Eq. (1)].

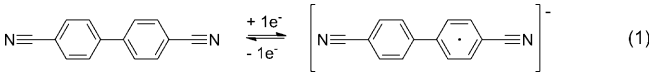

(1)

The second reduction wave is assigned to the formation of the dianion, followed by additional reactions [Eq. (2)].

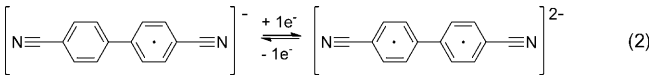

(2)

The first reduction process leading to the radical anions was investigated quantitatively. We estimated first the diffusion coefficients D_0 for the family of compounds **1–6** using Equation (3), in which n is the number of electrons in the redox process, F is the Faraday constant, A is the surface area of the electrode, C_0^* is the bulk concentration of the reactant, v is the scan rate, R is the universal gas constant and T is the absolute temperature.[42]

$$i = nFAC_0^*\sqrt{\left(\frac{D_0 nFv}{RT}\right)}\sqrt{\pi}\chi(at) \tag{3}$$

The parameter $\chi(at)$ is determined from the difference between the reduction peak potential and the potential of the half-wave, following the procedure in reference [42]. The diffusion coefficients obtained are rather similar, and range between 2.5×10^{-5} cm^{2}s^{-1} for **1** and 4.1×10^{-5} cm^{2}s^{-1} for **6**.

Using these values, we estimated the heterogeneous standard rate constants k_0 from Equation (4).[42]

$$\Psi = \frac{k_0}{\sqrt{D_0\pi\frac{nF}{RT}v}} \tag{4}$$

The kinetic parameter ψ is determined from the difference between the first reduction and the corresponding oxidation peak potentials. The smallest rate constant, $k_0 = 4.6\times10^{-3}$ cm s^{-1}, was found for **2** and **4**. The derivative with four CH_2 bridging units between the phenyl rings, led to the highest value of $k_0 = 1.0\times10^{-2}$ cm^{2}s^{-1}. Thus, the first electron-addition reaction is quasi-reversible for all the compounds studied.

In the following, we attempt to correlate the energetic data obtained from cyclic voltammetry and DFT with the torsion angle φ. We notice that the positions of the reduction peaks of both redox processes correlate linearly with the calculated LUMO energies (Figure S5 in the Supporting Information). The planar fluorene **1**, as well as compounds **2** and **5** with the least negative reduction potentials, are the best electron acceptors, and the tetramethyl compound **6** is the most difficult molecule to be reduced.

Moreover, the first and second reduction peaks of **1**, **2**, and **5** with torsion angles $\varphi \leq 39.60°$ appear at approximately the same potentials (Figure 7). Interestingly, very similar LUMO energies were also obtained for these structures in the DFT calculations (Figure S5 in the Supporting Information). It is worth noting that the first reduction wave of the planar fluorene **1** (1.02°) is slightly shifted to a more negative potential as compared to the nonplanar dihydrophenanthrene **2** (20.74°) and to compound **5** (39.60° (DFT)). The reduction potentials of **3**, **4**, and **6** shift significantly with increasing torsion angle φ ($\varphi > 39.60°$) towards more negative values. This trend directly reflects the order of calculated LUMO energies, as displayed in Figure 4. We note that no linear correlation between the positions of the individual redox peaks of the six model compounds and $\cos^2\varphi$ of the torsion angle was found (Figure S6 in the Supporting Information). However, the potential differences between the first and second reduction peaks (ΔE_{red}) exhibit a linear correlation with $\cos^2\varphi$ (Figure 8). Although the extent of electronic communication between the benzonitrile subunits is expected to increase with decreasing torsion angle φ, the obvious preservation of these structural features, even beyond the anion radical formation, is surprising.

The following scenario is suggested. The first one-electron transfer process leads to the formation of the radical anion [see Eq. (1)], in which the electric charge is partially delocalized on the π-system of one benzonitrile unit ("donor"), whereas the adjacent second benzonitrile unit remains un-

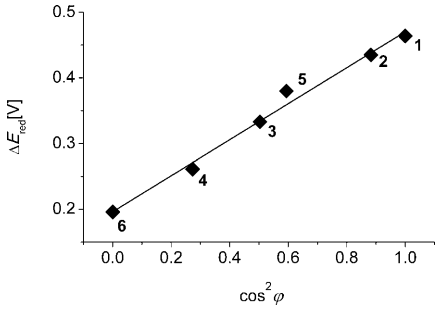

Figure 8. Linear correlation of the difference between the first and second reduction peaks (ΔE_{red}) with the $\cos^2\varphi$ (φ is the interplanar torsion angle obtained from the X-ray structures). The value for **5** was obtained from DFT calculations. The linear correlation coefficient R^2 is 0.986.

charged ("acceptor"). The π–π electronic coupling of the adjacent phenyl rings approximately follows the cosine of the torsion angle φ between them.[40b] The "rate constant" of the "donor"–"acceptor" electron transfer is proportional to the square of the coupling between the "donor" and "acceptor" rings.[44] These back-and-forth electron donations lead to the delocalization of electrons over the entire biphenyl π-system. As a consequence, the extent of the π-electron delocalization (electron mobility) is linearly proportional to $\cos^2\varphi$.

The subsequent addition of a second electron (during the second one-electron transfer process) onto the charged radical anion leads to a Coulomb repulsion between the two charges. Hence, the more the first electron is already delocalized over both benzonitrile subunits, the larger the repulsion for the addition of the second electron. Consequently, the potential difference between the first and second reduction peaks (ΔE_{red}) increases linearly with $\cos^2\varphi$ (Figure 8).

The model compound **6** (89.26°) with the two benzonitrile units perpendicular to one another displays a fully decoupled π-system. Only a slightly increased energy is required for the addition of a second electron, as the first electron is localized on one benzonitrile subunit leaving the second one basically unaffected. In contrast, the planar fluorene compound **1** (1.02°) no longer has a divided π-system, so the addition of a second electron induces a strong Coulomb repulsion, leading to a large value of ΔE_{red}. This hypothesis is further supported by the large ΔE_{red} for DCB,[43b–e] which consists, similarly to fluorene, of only one fully delocalized π-system for the acceptance of two electrons.

Spectroelectrochemistry: All CVs were recorded in a custom-designed spectroelectrochemical cell (Figure S7 in the Supporting Information) with sample concentrations of dicyanobiphenyl derivatives of 0.5 mM or 0.1 mM. Their overall shapes were identical to the curves recorded in a macroscopic all-glass electrochemical cell (Figure S8 in the Supporting Information shows a representative example for molecule **3**). Figure 9 shows the UV/Vis spectra recorded before the first redox process ($E=-0.2$ V) and at the potentials of the first reduction peak for a sample concentration of 0.1 mM. The spectra of the uncharged species (black lines) are identical to the traces plotted in Figure 5. Spectra during the first reduction process were recorded while maintaining the potential at the first reduction peak constant.

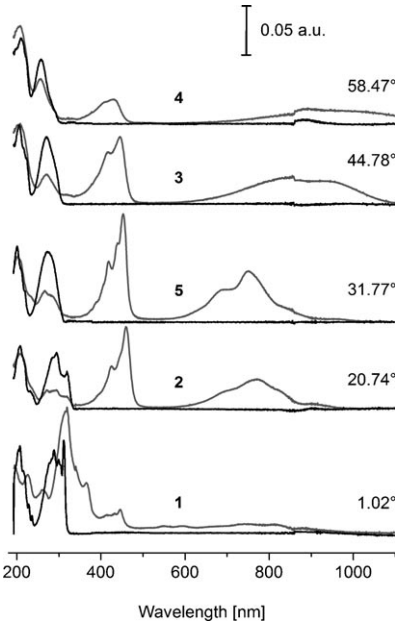

Figure 9. Spectroelectrochemical investigation of the dicyanobiphenyl compounds **1**–**5**. UV/Vis spectra with 0.1 mM sample concentrations in 0.1 M TBA·PF_6/CH_3CN electrolyte solution at −0.2 V (black lines) and at the potential of the first reduction peak maximum (gray lines).

We note that the limited cathodic stability of the Au/electrolyte system prevented us from reliably recording the spectroelectrochemical data of **6**.

The formation of the radical anions of model compounds **2** to **5** is represented by the evolution of two new spectral features at ≈450 nm and ≈600–1100 nm (gray lines). Simultaneously, the absorption band around 260–290 nm (black lines) decreases with time because of the reduction of the uncharged species. The current observed during the electrode polarization remains rather high; this is because of the continuous formation of the radical anion and its diffusion from the electrode surface into the electrolyte.

The radical anion is oxidized to the neutral species upon changing the potential back to the positive direction (−0.2 V). This is reflected by the decrease of the absorption bands above 400 nm, and by the reappearance of the initial spectra recorded at −0.2 V. Thus, the anion radicals are reversibly and completely oxidized back to the neutral compound at the electrode surface.

During the formation of the anion radical, an additional electron occupies the LUMO of the neutral molecule, which then becomes a SOMO (singly occupied MO).[45] Thus, the smaller excitation energies in the case of radical anions as compared with the neutral molecules correspond to transitions from the SOMO to the unoccupied orbitals (B_i type) and also from the filled orbitals to the SOMO (A_i type).

It is interesting to note that the position of the peak at ≈450 nm is shifted hypsochromically with increasing torsion angle φ for compounds **2**–**4** (gray lines in Figure 9). This follows the trend observed for the absorption bands at 240–295 nm (black lines in Figures 9 and 5) of the neutral molecules. In contrast, with increasing torsion angle φ, a bathochromic shift is observed for the band at 600–1100 nm.

The assignment of the energetic transitions observed is based on recent work by Nelsen et al.[45b] These authors investigated the optical spectra of dinitro-aromatic anion radicals including 4,4′-dinitrobiphenyl (4,4′-BI$^-$), which has a strong structural similarity with compound **5** of the present work. It consists of a biphenyl backbone with terminal nitro groups as strong electron acceptors. The use of Koopmans-based calculations allowed the authors to assign the peak at ≈455 nm in the UV/Vis spectrum of the 4,4′-BI$^{\bullet-}$ anion radical to the A_i (HOMO–SOMO) transition and the peaks at $\lambda > 500$ nm to B-type transitions. In analogy, we propose A-type transitions for the peaks at around 450 nm of the anion radicals of the dicyanobiphenyls studied here, and B-type transitions for peaks at longer wavelengths.

On the basis of this assignment, we explain the hypsochromic and bathochromic shifts of the peaks at ≈450 nm and around 600–1100 nm, respectively, caused by the increasing torsion angle φ, as follows. The HOMO–SOMO gap increases with increasing the torsion angle, whereas the gaps between the unoccupied orbitals and the SOMO decrease. Interestingly, even though the charging by an additional electron affects the energy-level diagram, these trends also correlate with the HOMO–LUMO and LUMO–LUMO+1 energy separations as calculated for the neutral molecules (see Figure 4).

The spectrum for the radical anion of **1** represents an exception, with an intense band at 320 nm, a less intense band at 446 nm, and a very broad feature at 500–900 nm.

We also tried to record UV/Vis spectra at the second reduction potential. However, the spectra were not reproducible and not reversible. After polarization at the potentials of the second reduction processes, the steady-state spectrum of the neutral compound (for instance at $E = -0.2$ V) was no longer observed. Additional shoulders appeared for all model compounds at 300–400 nm. Their intensities increased with the polarization time at potentials close to the second reduction peak, indicating follow-up and decomposition reactions of the charged species. The exact identification of these processes was beyond the scope of the present paper.

Conclusion

A series of dicyanobiphenyls **1**–**6** with various torsion angles φ between the phenyl rings were designed and synthesized as model compounds for the investigation of electron delocalization within gradually divided π-systems. The new structures were fully characterized; in particular, X-ray crystal analysis was used to document the gradual increase of the torsion angle with increasing length of the alkyl chain interlinking the biphenyl system in the 2- and 2′-positions. The extent of electron delocalization on the biphenyl backbone was investigated by UV/Vis spectroscopy, electrochemistry, and spectroelectrochemistry. Particular spectral features (such as the conjugation band in the series of absorption spectra, or the potential difference between the reduction peaks in the series of CVs) correlate with the $\cos^2$ value of the torsion angle. Interestingly, spectroelectrochemical investigations suggest that the separation of the π-systems within these biphenyls is maintained even beyond the radical anion.

In summary, these correlations demonstrate that the fixed intramolecular torsion angle φ is the dominant factor in determining the extent of electron delocalization in these model compounds, and that the angle φ measured in the solid-state structure is a good proxy for the molecular conformation in solution. The results are also supported by quantum mechanical investigations based on density functional theory.

Furthermore, these new biphenyl model compounds, with fixed backbone conjugation comprising terminal cyano groups, are promising candidates for single-molecule transport investigations.[7]

Experimental Section

General methods: All chemicals were used directly in the syntheses without purification unless otherwise indicated. All reactions were performed under argon with oven-dried glassware. ^{1}H and ^{13}C NMR spectra were recorded with a Bruker DPX-400 or Lambda-900 or -250 spectrometer. ^{1}H NMR chemical shifts are internally referenced to the residual solvent proton resonance ($CDCl_3$: $\delta = 7.26$ ppm; [D_6]DMSO: $\delta = 2.49$ ppm; CD_3CN: $\delta = 1.94$ ppm). ^{13}C NMR chemical shifts are internally referenced to the deuterated solvent signal ($CDCl_3$: $\delta = 77.2$ ppm; [D_6]DMSO: $\delta = 39.7$ ppm; CD_3CN: $\delta = 118.3$ ppm, $\delta = 1.8$). Mass spectra were recorded with an Esquire 3000 plus (Bruker) for electron spray ionization (ESI) MS or with a Finnigan MAT 95Q spectrometer for electron impact (EI) MS. Elemental analyses were carried out with a Perkin–Elmer Analyser 240. Flash chromatography was performed on silica gel 60 (40–63 μm) from Merck.

Voltammetric and spectroelectrochemical measurements: Electrochemical experiments were performed in an electrochemical glass cell (the volume of the solution was 1 mL). In all experiments we used 0.1 M TBA·PF_6 (Fluka, puriss, electrochemical grade) in CH_3CN (ACROS organics, HPLC) as supporting electrolyte. A Pt wire and an assembly of Ag/0.01 M $AgNO_3$ + 0.1 M TBA·PF_6 in CH_3CN served as the counter and reference electrodes, respectively. The electrochemical measurements were carried out on Au net (Figure S7 in the Supporting Information) and glassy carbon working electrodes. To calibrate the potential, we added 0.5 mM ferrocene to the cell as a standard, and recorded cyclic voltammograms at the end of each experiment. UV/Vis spectra were recorded under potential control using the optical cell shown in Figure S7 of the Supporting Information. The working electrode was a gold net, and the counter and reference electrodes were the same as in the electrochemical cell. Ar was passed over the solution in the cell during all experiments. Ar was saturated with CH_3CN before being introduced into the cell to prevent evaporation of the solvent. Before every experiment, the Au net was cleaned in caroic acid, rinsed with ultrapure water, and dried in a strong Ar stream. The GC electrode was polished with 0.05 μm aluminum paste, thoroughly rinsed with water using an ultrasonic bath, and then dried in an Ar stream. The Pt counter electrode was flame-annealed before each use.

Synthesis:

*4,4′-Dimethoxy-2,2-dimethylbiphenyl (**7**)*: Under an inert atmosphere, 1-bromo-4-methoxy-2-methylbenzene (34.90 g, 0.174 mol) was dropped into a suspension of magnesium (6.10 g, 0.251 mol, 1.4 equiv) in dry methyltetrahydrofuran (MeTHF, 150 mL) at such a rate that the moderate conversion of the halogenide was maintained. Then the reaction mixture was heated at reflux for 30 min and cooled to room temperature. The Grignard reagent was slowly transferred to a refluxing solution of 1,2-dichloroethane (23 mL, 0.292 mol, 1.7 equiv) and anhydrous $FeCl_3$ (2.00 g, 12.33 mmol, 7.1 mol%) in dry diethyl ether (250 mL). The reaction mixture was heated under reflux for 70 min, cooled to room temperature, and poured onto ice. Then, HCl (20 mL, 37%) was added, the organic layer was separated, and the aqueous phase was extracted with methyl *tert*-butyl ether (*t*BME, 3×50 mL). The combined extracts were washed with NaOH (2×50 mL, 1.0 M) and filtered through a silica pad. The colorless oil was dried in vacuo to afford **7** (19.40 g, 80.06 mmol, 92%), which was pure enough to be used in the next step without further purification. For analytical purposes, flash chromatography was performed (silica, CH_2Cl_2 in hexane, 20–100%). ^{1}H NMR (400 MHz, $CDCl_3$, 25 °C): δ = 2.06 (s, 6H), 3.85 (s, 6H), 6.78 (dd, ^3J(H,H) = 8.3, ^4J(H,H) = 2.5, 2H), 6.84 (d, ^4J(H,H) = 2.5 Hz, 2H), 7.03 ppm (d, ^3J(H,H) = 8.3, 2H); ^{13}C NMR (100 MHz, $CDCl_3$, 25 °C): δ = 20.6, 55.6, 111.2, 115.6, 131.1, 134.2, 138.1, 159.0 ppm; MS (70 eV): *m/z* (%): 242.1 (100) [M^+]; elemental analysis calcd (%) for $C_{16}H_{18}O_2$: C 79.31, H 7.49; found: C 78.14, H 7.26.

*2,2′-Bis(bromomethyl)-4,4′-dimethoxybiphenyl (**8**)*: NBS (3.10 g, 17.41 mmol, 2.1 equiv) and benzoyl peroxide (0.20 g, 0.62 mmol, 7.5 mol%, 75%) were added to a solution of **7** (2.00 g, 8.25 mmol) in CCl_4 (60 mL). The reaction was kept at reflux until all starting material was converted (GC-MS, 2 h). The cooled reaction mixture was filtered through a silica pad and the solvent was evaporated. Flash chromatography was performed (silica, CH_2Cl_2 in hexane, 30–90%) to afford pure 2,2′-bis(bromomethyl)-4,4′-dimethoxy-biphenyl **8** (2.23 g, 5.57 mmol, 68%) as a thick colorless oil that solidified upon standing. M.p. 75 °C; ^{1}H NMR (250 MHz, $CDCl_3$, 25 °C): δ = 3.87 (s, 6H), 4.17 (d, ^2J(H,H) = 9.9 Hz, 2H), 4.31 (d, ^2J(H,H) = 9.9 Hz, 2H), 6.91 (dd, ^3J(H,H) = 8.4, ^4J(H,H) = 2.7 Hz, 2H), 7.06 (d, 7.18, ^4J(H,H) = 2.7 Hz, 2H), 7.18 ppm (d, ^3J(H,H) = 8.4 Hz, 2H); ^{13}C NMR (100 MHz, $CDCl_3$, 25 °C): δ = 32.6, 55.8, 114.7, 115.8, 131.9, 132.1, 137.9, 159.8 ppm; MS (70 eV): *m/z* (%): 398.0 (50), 400.0 (100), 402.0 (49) [M^+]; HRMS (ESI): *m/z* calcd for $C_{16}H_{16}O_2Br_2$ [M+Na]$^+$: 420.9416; found: 420.9414; elemental analysis calcd (%) for $C_{16}H_{16}Br_2O_2$: C 48.03, H 4.03; found: C 47.94, H 3.91.

*3,9-Dimethoxy-5,7-dihydrodibenzo[a,c]cyclohepten-6-one (**9**)*: Under ice cooling, NaOH (294 mg, 7.35 mmol, 5.0 equiv) was dissolved in H_2O (4 mL) and added to a suspension of **8** (589 mg, 1.47 mmol), toluenesulfonylmethyl isocyanide (287 mg, 1.47 mmol, 1.0 equiv), and tetrabutylammonium bromide (TBAB, 30 mg, 93 μmol, 6.3 mol%) in CH_2Cl_2 (10 mL). The two-phase mixture was stirred vigorously at room temperature overnight. *t*BME (16 mL) and HCl (8 mL, 37%) were added, and the mixture was stirred for 3 h. The phases were separated and the organic layer was washed with saturated $NaHCO_3$, dried over $MgSO_4$, and the solvent was evaporated. The crude product was purified by flash chromatography (silica, CH_2Cl_2) to afford **9** as a white solid (326 mg, 1.22 mmol, 83%). M.p. 126 °C; ^{1}H NMR (250 MHz, $CDCl_3$, 25 °C): δ = 3.45 (d, ^2J(H,H) = 13.0 Hz, 2H), 3.59 (d, ^2J(H,H) = 13.0 Hz, 2H), 6.79 (d, ^4J(H,H) = 2.6 Hz, 2H), 6.94 (dd, ^3J(H,H) = 8.5, ^4J(H,H) = 2.6 Hz, 2H), 7.44 ppm (d, ^3J(H,H) = 8.5 Hz, 2H); ^{13}C NMR (100 MHz, $CDCl_3$, 25 °C): δ = 50.0, 55.8, 113.7, 114.9, 130.6, 132.1, 134.3, 159.4, 210.5 ppm; MS (70 eV): *m/z* (%): 268.1 (100) [M^+], 225.1 (67), 165.1 (15), 153.1 (11); HRMS (ESI): *m/z* calcd for $C_{17}H_{16}O_3$ [M+Na]$^+$: 291.0997; found: 291.0993.

*3,9-Dimethoxy-6,7-dihydro-5 H-dibenzo[a,c]cycloheptene (**10**)*: Hydrazine monohydrate (0.35 mL, 7.21 mmol, 2.3 equiv) was added to a suspension of **9** (854 mg, 3.18 mmol) and powdered KOH (750 mg, 13.37 mmol, 4.2 equiv) in diethylene glycol (10 mL) under ice cooling. The mixture was heated to reflux for 2 h. The water and excess of hydrazine was distilled off at an oil-bath temperature of 190 °C. After a total reaction time of 3 h and a maximum oil-bath temperature of 195 °C, the reaction was stopped. Water (40 mL) was added to the cooled reaction mixture, followed by extraction with *t*BME (4×20 mL). The combined organic layers were washed with HCl (1×20 mL, 1.0 M), water (3×10 mL), and brine (1×30 mL), dried over $MgSO_4$, and filtered through a short silica pad. After evaporation of the solvent, **10** (700 mg, 2.75 mmol, 86%) was obtained as a white oil that solidified upon standing. M.p. 110 °C; ^{1}H NMR (250 MHz, $CDCl_3$, 25 °C): δ = 2.16 (m, 2H), 2.47 (m, 4H), 7.19 (d, ^4J(H,H) = 2.4 Hz, 2H), 7.27 (dd, ^3J(H,H) = 8.4, ^4J(H,H) = 2.6 Hz, 2H), 7.41 ppm (d, ^3J(H,H) = 8.4 Hz, 2H); ^{13}C NMR (100 MHz, $CDCl_3$, 25 °C): δ = 32.2, 33.3, 55.7, 111.9, 114.6, 129.5, 133.9, 141.3, 159.1 ppm; HRMS (ESI): *m/z* calcd for $C_{17}H_{19}O_2$ [M+Na]$^+$: 255.1385; found: 255.1385.

*3,9-Dihydroxy-6,7-dihydro-5 H-dibenzo[a,c]cycloheptene (**11**)*: The dimethoxy compound **10** was deprotected with BBr_3 according to the protocol to afford **16**. The crude diol **11** was obtained as a white powder, which was used without further purification for the next step. ^{1}H NMR (250 MHz, $CDCl_3$, 25 °C): δ = 2.14 (m, 2H), 2.44 (m, 4H), 4.66 (brs, 2H), 6.72 (d, ^4J(H,H) = 2.4 Hz, 2H), 6.78 (dd, ^3J(H,H) = 8.0, ^4J(H,H) = 2.4 Hz, 2H), 7.19 ppm (d, ^3J(H,H) = 8.0 Hz, 2H); ^{13}C NMR (100 MHz, $CDCl_3$, 25 °C): δ = 31.5, 32.7, 113.0, 115.2, 128.9, 132.6, 140.7, 155.4 ppm; MALDI-TOF MS (without matrix): *m/z* = 226.4 [M^+].

*3,9-Bis-(trifluoromethanesulfonyloxy)-6,7-dihydro-5 H-dibenzo-[a,c]cycloheptene (**12**)*: The crude diol **11** was esterified with triflic anhydride and pyridine as the base, according to the known protocol.[11a] The ditriflate **12** was obtained as a colorless oil. The yield over two steps was 84%. ^{1}H NMR (250 MHz, $CDCl_3$, 25 °C): δ = 2.24 (m, 2H), 2.52 (m, 4H), 7.19 (d, ^4J(H,H) = 2.5 Hz, 2H), 7.27 (dd, ^3J(H,H) = 8.4, ^4J(H,H) = 2.5 Hz, 2H), 7.41 ppm (d, ^3J(H,H) = 8.4 Hz, 2H); ^{13}C NMR (100 MHz, $CDCl_3$, 25 °C): δ = 31.2, 32.6, 119.6, 121.4, 130.0, 139.6, 142.1, 149.0 ppm; ^{19}F NMR: δ = −74.0 ppm; MS (70 eV): *m/z* (%): 490.0 (37) [M^+]; elemental analysis calcd (%) for $C_{17}H_{12}F_6O_6S_2$: C 41.64, H 2.47; found: C 41.72, H 2.48.

*Representative example for cyanation method A—3,9-dicyano-6,7-dihydro-5 H-dibenzo[a,c]cycloheptene (**3**)*: Potassium cyanide (100 mg, 1.54 mmol, 3.0 equiv), $Pd_2(dba)_3{\cdot}CHCl_3$ (53 mg, 51 μmol, 10.0 mol%), and xantphos (30 mg, 51 μmol, 10.0 mol%) were added to a solution of **12** (251 mg, 0.51 mmol) in dry and degassed acetonitrile (5 mL). Tributyltin chloride (3.9 μL, 14.4 μmol, 2.8 mol%) was added, and the reaction mixture was heated at reflux for 16 h, then cooled to room temperature; the solvent was evaporated, and the dicyano compound **3** was purified by flash chromatography (silica, CH_2Cl_2) to obtain a white solid. Recrystallization from a mixture of hot dioxane and cyclohexane using the slow evaporation technique gave single crystals suitable for X-ray analysis (102 mg, 0.418 mmol, 82%). M.p. 246–248 °C; ^{1}H NMR (400 MHz, $CDCl_3$, 25 °C): δ = 2.21–2.29 (m, 2H), 2.52 (brs, 4H), 7.45 (d, ^3J(H,H) = 7.9 Hz, 2H), 7.57 (d, ^4J(H,H) = 1.6 Hz, 2H), 7.67 ppm (dd, ^3J(H,H) = 8.1, ^4J(H,H) = 1.6 Hz, 2H); ^{13}C NMR (100 MHz, $CDCl_3$, 25 °C): δ = 31.2, 33.1, 112.7, 119.1, 129.4, 131.2, 132.6, 141.1, 144.3 ppm; MS (70 eV): *m/z* (%): 244.1 (100) [M^+], 229.1 (74), 216.1 (26), 202.1 (11); elemental analysis calcd (%) for $C_{17}H_{12}N_2$: C 83.58, H 4.95, N 11.47; found: C 83.45, H 5.14, N 11.39.

*2,2′-Diallyl-4,4′-dimethoxybiphenyl (**13**)*: Compound **8** (4.00 g, 10.00 mmol) was dissolved in dry CH_2Cl_2 (15 mL) and added to a vinyl magnesium bromide solution in dry THF (86 mL, 60.20 mmol, 6.0 equiv, 0.7 M) at −50 °C. Then CuI (1.90 g, 10.00 mmol, 1.0 equiv) was added immediately and the reaction mixture was allowed to reach room temperature overnight. The black suspension was poured onto a cold NH_4Cl solution (300 mL). The organic layer was separated, and the aqueous phase was extracted with *t*BME (3×150 mL). The combined organic phases were washed with brine (150 mL), dried over $MgSO_4$, and filtered through celite. After evaporation of the solvent, flash chromatography (silica, hexane/CH_2Cl_2, 1:1) was performed to obtain **13** (2.27 g, 7.71 mmol, 77%) as a colorless smelly oil. ^{1}H NMR (400 MHz, $CDCl_3$, 25 °C): δ = 3.03–3.14 (m, 4H), 3.84 (s, 6H), 4.87–4.98 (m, 4H), 5.74–5.84, (m, 2H), 6.79 (dd, ^3J(H,H) = 8.3, ^4J(H,H) = 2.7 Hz, 2H), 6.83 (d, ^4J(H,H) = 2.7 Hz, 2H), 7.03 ppm (d, ^3J(H,H) = 8.3 Hz, 2H); ^{13}C NMR (100 MHz, $CDCl_3$, 25 °C): δ = 38.3, 55.6, 111.5, 114.9, 116.3, 131.7, 133.4, 137.5, 140.1, 159.2 ppm; MS (70 eV): *m/z* (%): 294.2 (100) [M^+]; elemental analysis calcd (%) for $C_{20}H_{22}O_2$: C 81.60, H 7.53; found: C 80.28, H

7.41; HRMS (ESI): *m/z* calcd for $C_{20}H_{22}O_2$ $[M+Na]^+$: 317.1517; found: 317.1512.

*3,10-Dimethoxy-5,8-dihydrodibenzo[a,c]cyclooctene (**14**)*: Compound **13** (1.84 g, 6.25 mmol) was dissolved in CH_2Cl_2 (500 mL). After addition of the Grubbs catalyst (1st Generation, 0.26 g, 0.32 mmol, 5.0 mol%) the solution was heated at reflux for 16 h and the solvent was evaporated. The product was purified by flash chromatography (silica, hexane/CH_2Cl_2, 1:1) to give **14** (1.32 g, 4.96 mmol, 79%) as a white solid. M.p. 142°C; ^{1}H NMR (400 MHz, $CDCl_3$, 25°C): δ=2.98–3.09 (m, 4H), 3.84 (s, 6H), 5.80–5.88 (m, 2H), 6.75 (d, ^4J(H,H)=2.7 Hz, 2H), 6.83 (dd, ^3J(H,H)=8.3, ^4J(H,H)=2.7 Hz, 2H), 7.17 ppm (d, ^3J(H,H)=8.3 Hz, 2H); ^{13}C NMR (100 MHz, $CDCl_3$, 25°C): δ=34.2, 55.7, 112.0, 114.8, 129.3, 129.4, 134.9, 138.7, 160.0 ppm; MS (70 eV): *m/z* (%): 266.1 (100) $[M^+]$; elemental analysis calcd (%) for $C_{18}H_{18}O_2$: C 81.17, H 6.81; found: C 80.72, H 6.84; HRMS (ESI): *m/z* calcd for $C_{18}H_{18}O_2$ $[M+Na]^+$: 289.1204; found: 289.1210.

*3,10-Dimethoxy-5,6,7,8-tetrahydrodibenzo[a,c]cyclooctene (**15**)*: Compound **14** (1.08 g, 4.06 mmol) was dissolved in ethyl acetate (70 mL), and Pd/C (120 mg, 10% Pd) was added. The mixture was stirred under a hydrogen atmosphere (1 atm) for 3 h. Then, the solution was filtered through a silica pad and the solvent was evaporated. **15** was collected as a white solid (1.07 g, 3.99 mmol, 98%). M.p. 152°C; ^{1}H NMR (400 MHz, $CDCl_3$, 25°C): δ=1.48–1.57 (m, 2H), 2.01–2.19 (m, 4H), 2.64–2.69 (m, 2H), 3.80 (s, 6H), 6.78–6.80 (m, 4H), 7.13–7.16 ppm (m, 2H); ^{13}C NMR (100 MHz, $CDCl_3$, 25°C): δ=30.1, 33.5, 55.7, 111.5, 114.8, 130.6, 133.5, 144.6, 159.5 ppm; MS (70 eV): *m/z* (%): 268.1 (100) $[M^+]$; elemental analysis calcd (%) for $C_{18}H_{20}O_2$: C 80.56, H 7.51; found: C 80.62, H 7.50.

*3,10-Dihydroxy-5,6,7,8-tetrahydrodibenzo[a,c]cyclooctene (**16**)*: BBr_3 (2.9 mL, 30.60 mmol, 5.5 equiv) was slowly dropped into a solution of **15** (1.50 g, 5.59 mmol) in dry CH_2Cl_2 (80 mL) at 0°C. Stirring was continued at room temperature until TLC showed full conversion of the starting material (1.5 h). The reaction was quenched with MeOH under ice cooling. The reaction mixture was washed with water (50 mL) and dried over $MgSO_4$, and the solvent was evaporated. The crude **16** (1.67 g) was obtained as a white powder which was pure enough to be used for the next step. Flash chromatography was performed (silica, hexane/*t*BME, 2:1) to obtain a sample for analytical purposes. M.p. 130–134°C; ^{1}H NMR (400 MHz, [D$_6$]DMSO, 25°C): δ=1.31–1.33 (m, 2H), 1.86–2.00 (m, 4H), 2.50–2.55 (m, 2H), 6.58–6.62 (m, 4H), 6.90 (d, ^3J(H,H)=8.0 Hz, 2H), 9.23 ppm (br s, 2H); ^{13}C NMR (100 MHz, $CDCl_3$, 25°C): δ=30.4, 33.4, 113.7, 116.3, 130.6, 131.9, 144.1, 157.5 ppm; MS (70 eV): *m/z* (%): 240.1 (100) $[M^+]$; HRMS (ESI): *m/z* calcd for $C_{16}H_{16}O_2$ $[M+Na]^+$: 263.1047; found: 263.1056.

*Bis-(trifluoromethanesulfonyloxy)-5,6,7,8-tetrahydro-dibenzo-[a,c]cyclooctene (**17**)*: The crude diol **16** was esterified with triflic anhydride and pyridine as the base according to a known protocol.[11] The ditriflate **17** was obtained as a colorless oil, which solidified upon standing (2.33 g, 4.62 mmol, 83% over two steps). M.p. 69–70°C; ^{1}H NMR (400 MHz, $CDCl_3$, 25°C): δ=1.48–1.53 (m, 2H), 2.08–2.15 (m, 4H), 2.74–2.79 (m, 2H), 7.16–7.21 (m, 4H), 7.29 ppm (d, ^3J(H,H)=8.3 Hz, 2H); ^{13}C NMR (100 MHz, $CDCl_3$, 25°C): δ=29.0, 32.6, 118.7, 119.2 (q, J(C,F)=319 Hz), 122.0, 130.6, 140.0 145.4, 149.5 ppm; ^{19}F NMR (376 MHz, $CDCl_3$, 25°C): δ=−74.0 ppm; MS (70 eV): *m/z* (%): 504.0 $[M^+]$; elemental analysis calcd (%) for $C_{18}H_{14}F_6O_2S_2$: C 42.86, H 2.80; found: C 42.91, H 2.75.

*3,10-Dicyano-5,6,7,8-tetrahydrodibenzo[a,c]cyclooctene (**4**)*: The triflate **17** was converted to the dicyanide **4** according to *method A* (see synthetic protocol for **3**). The dicyanide **4** was purified by flash chromatography (silica, CH_2Cl_2/hexane, 8:2) to give a white solid. Recrystallization from a mixture of hot dioxane and cyclohexane using the slow evaporation technique gave single crystals suitable for the X-ray analysis (132 mg, 0.51 mmol, 86%). M.p. 248–249°C; ^{1}H NMR (400 MHz, $CDCl_3$, 25°C): δ=1.45–1.53 (m, 2H), 2.04–2.18 (m, 4H), 2.75–2.82 (m, 2H), 7.31 (d, ^3J(H,H)=7.9 Hz, 2H), 7.57 (dd, ^3J(H,H)=7.9, ^4J(H,H)=1.6 Hz, 2H), 7.61 ppm (d, ^3J(H,H)=7.9 Hz, 2H); ^{13}C NMR (100 MHz, $CDCl_3$, 25°C): δ=29.3, 32.6, 113.1, 119.1, 129.9, 130.0, 133.7, 143.8, 144.2 ppm; MS (70 eV): *m/z* (%): 258.1 $[M^+]$, 243.1 (18), 229.1 (67), 216.1 (35), 202.1 (15), 190.1 (14); elemental analysis calcd (%) for $C_{18}H_{14}N_2$: C 83.69, H 5.46, N 10.84; found: C 83.37, H 5.54, N 10.82.

*Representative example for cyanation method B—4,4′-dicyanobiphenyl (**5**)*: Copper(I) cyanide (0.860 g, 9.62 mmol, 3.0 equiv) was dried under high vacuum. Then, the copper salt and **20** (1.00 g, 3.20 mmol) were suspended in dry DMF, and the reaction mixture was stirred at 150–160°C for 16 h. The reaction mixture was cooled to room temperature, water (80 mL) and ethylenediamine (10 mL) were added, and the mixture was stirred at 70°C for 10 min and cooled again to room temperature. The dark blue reaction mixture was extracted with CH_2Cl_2. The organic phase was washed with water and brine, dried over $MgSO_4$, and evaporated on a rotary evaporator. The residue was taken up in hot EtOH/water and cooled to room temperature. The powder was filtered off and dried in vacuo. Compound **5** was obtained as a beige powder (480 mg, 2.35 mmol, 73%). Chromatographic purification (silica, CH_2Cl_2) of **5** was achieved by dissolving the compound in a large amount of chloroform and adsorbing it to the immobilized phase. This was followed by recrystallization from a hot mixture of dioxane and cyclohexane using the slow evaporation technique, affording single crystals suitable for X-ray analysis. M.p. 227–239°C; ^{1}H NMR (250 MHz, [D$_6$]DMSO, 25°C): δ=7.81–7.87 ppm (m, 8H); ^{13}C NMR (100 MHz, $CDCl_3$, 25°C): δ=112.9, 118.3, 119.4, 129.0, 133.9 ppm; MS (70 eV): *m/z* (%): 204.1 (100) $[M^+]$; elemental analysis calcd (%) for $C_{14}H_8N_2$: C 82.34, H 3.95, N 13.72; found: C 82.07, H 4.17, N 13.75.

*2,7-Dicyanofluorene (**1**)*: Cyclophane **1** was obtained from the commercially available **18** according to *method B*. The reaction time was 6 h. 2.6 equivalents of copper(I) cyanide were used, and the product was extracted several times with ethyl acetate. The combined extracts were filtered through a silica pad, and the solvent was evaporated on the rotary evaporator. The beige residue was repeatedly recrystallized from hot acetonitrile, ethanol, and methoxyethanol. **1** (540 mg, 2.49 mmol, 51%) was obtained as fine yellow crystals. For the elemental analysis, a final chromatographic purification of **1** was achieved by dissolving the compound in a large amount of chloroform and adsorbing it to silica (eluent: CH_2Cl_2). This was followed by recrystallization from a hot mixture of dioxane and cyclohexane, affording single crystalline material suitable for X-ray analysis and for carrying out all analytical tests. M.p. 279–281°C; ^{1}H NMR (400 MHz, $CDCl_3$, 25°C): δ=4.04 (s, 2H), 7.74 (dd, ^3J(H,H)=8.0, ^4J(H,H)=1.3 Hz, 2H), 7.89 (d, ^3J(H,H)=8.0 Hz, 2H), 7.93 ppm (dd, ^3J(H,H)=8.0 Hz, 2H); ^{13}C NMR (100 MHz, $CDCl_3$, 25°C): δ=37.12, 112.06, 119.42, 121.97, 129.37, 131.94, 144.54, 144.62 ppm; MS (70 eV): *m/z* (%): 216.1 (100) $[M^+]$; elemental analysis calcd (%) for $C_{15}H_8N_2$: C 83.32, H 3.73, N 12.95; found: C 83.35, H 3.91, N 12.83.

*2,7-Dicyano-9,10-dihydrophenanthrene (**2**)*: Dicyanide **2** was obtained according to *method B* from dibromide[19] **19**. The reaction time was 18 h. The obtained beige powder containing traces of DMF was recrystallized from hot toluene to give **2** (360 mg, 1.56 mmol, 53%) as fine yellow crystals. Subsequent recrystallization from a boiling mixture of dioxane and cyclohexane gave **2** as a colorless prism suitable for X-ray measurements. M.p. 299–300°C; ^{1}H NMR (400 MHz, $CDCl_3$, 25°C): δ=2.94 (s, 4H), 7.57 (d, ^3J(H,H)=8.1 Hz, 2H), 7.64 (dd, ^3J(H,H)=8.1, ^4J(H,H)=1.4 Hz, 2H), 7.83 ppm (d, ^3J(H,H)=8.1 Hz, 2H); ^{13}C NMR (100 MHz, $CDCl_3$, 25°C): δ=28.44, 112.48, 119.02, 125.39, 131.50, 132.31, 137.49, 139.10 ppm; MS (70 eV): *m/z* (%): 230.1 (100) $[M^+]$, 215.1 (16), 202.1 (14), 190.1 (26); elemental analysis calcd (%) for $C_{16}H_{10}N_2$: C 83.46, H 4.38, N 12.17; found: C 83.19, H 4.56, N 12.15.

*4,4′-Dicyano-2,2′,6,6′-tetramethylbiphenyl (**6**)*: Dicyanide **6** was obtained according to *method B*, starting from 4,4′-diiodo-2,2′,6,6′-tetramethylbiphenyl **21**.[11a] The reaction was completed within 8 h at 140°C. The cyano compound **6** was purified by flash chromatography (silica, CH_2Cl_2/hexane, 8:2), affording an off-white crystalline powder (344 mg, 1.32 mmol, 84%). Recrystallization using the slow evaporation technique (cyclohexane) gave single crystals suitable for X-ray analysis. M.p. 249–250°C; ^{1}H NMR (400 MHz, $CDCl_3$, 25°C): δ=1.91 (s, 12H), 7.46 ppm (s, 4H); ^{13}C NMR (100 MHz, $CDCl_3$, 25°C): δ=19.94, 112.15, 119.22, 131.81, 137.03, 143.68 ppm; MS (70 eV): *m/z* (%): 260.1 (62) $[M^+]$; elemental analysis calcd (%) for $C_{18}H_{16}N_2$; C 83.04, H 6.19, N 10.76; found: C 83.03, H 6.40, N 10.74.

Acknowledgements

The authors acknowledge the support of the Swiss National Science Foundation for the National Research Program 62 "Smart Materials", the Sinergia Program "Electromechanical Systems and the Swiss National Center of Competence in Research "Nanoscale Science" and of the ITN FP7 network FUNMOLS. The authors are grateful to Dr. Fabian Pauly and Carmen Blum for helpful discussions.

[1] a) A. Facchetti, *Mater. Today* **2007**, *10*, 28–37; b) T. Mori, *J. Phys. Condens. Matter* **2008**, *20*, 184010; c) G. Horowitz, *Adv. Mater.* **1990**, *2*, 287–292.

[2] a) N. Blouin, M. Leclerc, *Acc. Chem. Res.* **2008**, *41*, 1110–1119; b) M. He, J. Li, M. L. Sorensen, F. Zhang, R. R. Hancock, H. H. Fong, V. A. Pozdin, D.-M. Smilgies, G. G. Malliaras, *J. Am. Chem. Soc.* **2009**, *131*, 11930–11938.

[3] a) D. Vonlanthen, A. Mishchenko, M. Elbing, M. Neuburger, T. Wandlowski, M. Mayor, *Angew. Chem.* **2009**, *121*, 9048–9052; *Angew. Chem. Int. Ed.* **2009**, *48*, 8886–8890; b) A. Mishchenko, D. Vonlanthen, V. Meded, M. Bürkle, C. Li, I. V. Pobelov, A. Bagrets, J. K. Viljas, F. Pauly, F. Evers, M. Mayor, T. Wandlowski, *Nano Lett.* **2010**, *10*, 156–163; c) L. Venkataraman, J. E. Klare, C. Nuckolls, M. S. Hybertsen, M. L. Steigerwald, *Nature* **2006**, *442*, 904–907.

[4] a) C. R. Newman, C. D. Frisbie, D. A. da Silva Filho, J.-L. Brédas, P. C. Ewbank, K. R. Mann, *Chem. Mater.* **2004**, *16*, 4436–4451; b) Y. Didane, P. Marsal, F. Fages, A. Kumagai, N. Yoshimoto, H. Brisset, C. Videlot-Ackermann, *Thin Solid Films* **2010**, *519*, 578–586.

[5] a) H. E. Katz, A. J. Lovinger, J. Johnson, C. Kloc, T. Siegrist, W. Li, Y. Y. Lin, A. Dodabalapur, *Nature* **2000**, *404*, 478–481; b) H. E. Katz, J. Johnson, A. J. Lovinger, W. Li, *J. Am. Chem. Soc.* **2000**, *122*, 7787–7792.

[6] K. Becker, E. Da Como, J. Feldmann, F. Scheliga, E. Thorn Csanyi, S. Tretiak, J. M. Lupton, *J. Phys. Chem. B* **2008**, *112*, 4859–4864.

[7] A. Mishchenko, L. Zotty, D. Vonlanthen, J. C. Cuevas, M. Bürkle, F. Pauly, M. Mayor, T. Wandlowski, *J. Am. Chem. Soc.* **2011**, *133*, 184–187.

[8] A. Ulman in *Self-Assembled Monolayers of Thiols (Thin Films), Vol. 24* (Ed.: R. Powell, M. H. Francombe, A. Ulman), Academic Press, San Diego, **1998**, p. 278.

[9] S. Y. Quek, L. Venkataraman, H. J. Choi, S. G. Louie, M. S. Hybertsen, J. B. Neaton, *Nano Lett.* **2007**, *7*, 3477–3482.

[10] a) J. Casanova Jr. , N. D. Werner, R. E. Schuster, *J. Org. Chem.* **1966**, *31*, 3473–3482; b) J. Sun, X. Qian, D. Chen, Y. Liu, D. Wang, Q. Chang, *J. Photochem. Photobiol. A* **1999**, *126*, 23–26.

[11] a) D. Vonlanthen, J. Rotzler, M. Neuburger, M. Mayor, *Eur. J. Org. Chem.* **2010**, 120–133; b) J. Rotzler, D. Vonlanthen, A. Barsella, A. Boeglin, A. Fort, M. Mayor, *Eur. J. Org. Chem.* **2010**, 1096–1110.

[12] a) T. Nagano, T. Hayashi, *Org. Lett.* **2005**, *7*, 491–493; b) G. Cahiez, C. Chaboche, F. Mahuteau-Betzer, M. Ahr, *Org. Lett.* **2005**, *7*, 1943–1946.

[13] O. Possel, A. M. van Leusen, *Tetrahedron Lett.* **1977**, *18*, 4229–4231.

[14] R. W. McDonald, W. Bunjobpon, T. Liu, S. Fessler, O. E. Pardo, I. K. Freer, M. Glaser, M. J. Seckl, D. J. Robins, *Anti-Cancer Drug Des.* **2001**, *16*, 261–270.

[15] a) C. Yang, J. M. Williams, *Org. Lett.* **2004**, *6*, 2837–2840; b) M. P. Wentland, R. Lou, Q. Lu, Y. Bu, M. A. VanAlstine, D. J. Cohen, J. M. Bidlack, *Bioorg. Med. Chem. Lett.* **2009**, *19*, 203–208; c) L. S. Suwandi, G. E. Agoston, J. H. Shah, A. D. Hanson, X. H. Zhan, T. M. LaVallee, A. M. Treston, *Bioorg. Med. Chem. Lett.* **2009**, *19*, 6459–6462.

[16] W.-F. Jiang, H.-L. Wang, A.-G. Wang, Z.-Q. Li, *Synth. Commun.* **2008**, *38*, 1888–1895.

[17] J. Lindley, *Tetrahedron* **1984**, *40*, 1433–1456.

[18] a) J. A. J. Vink, P. L. Verheijdt, J. Cornelisse, E. Havinga, *Tetrahedron* **1972**, *28*, 5081–5087; b) M. Minabe, K. Suzuki, *Bull. Chem. Soc. Jpn.* **1972**, *45*, 3196–3201; c) G. Kossmehl, K.-H. Hatscher, G. Manecke, *Makromol. Chem.* **1975**, *176*, 539–559; d) J. Spychala, *Monatsh. Chem.* **2006**, *137*, 1203–1210.

[19] A. D. Abell, M. Brandt, M. A. Levy, D. A. Holt, *J. Chem. Soc. Perkin Trans. 1* **1997**, 1663–1668.

[20] A. T. H. Lenstra, C. VanAlsenoy, K. Verhulst, H. J. Geise, *Acta Crystallogr. Sect. B* **1994**, *50*, 96–106.

[21] a) F. Leroux, *ChemBioChem* **2004**, *5*, 644–649; b) A. Mazzanti, L. Lunazzi, M. Minzoni, J. E. Anderson, *J. Org. Chem.* **2006**, *71*, 5474–5481.

[22] a) K. Müllen, W. Heinz, F.-G. Klärner, W. R. Roth, I. Kindermann, O. Adamczak, M. Wette, J. Lex, *Chem. Ber.* **1990**, *123*, 2349–2371; b) J. Rotzler, H. Gsellinger, M. Neuburger, D. Vonlanthen, D. Häussinger, M. Mayor, *Org. Biomol. Chem.* , **2011**, *9*, 86–91.

[23] F. Grein, *J. Phys. Chem. A* **2002**, *106*, 3823–3827.

[24] a) P. A. Wood, S. J. Borwick, D. J. Watkin, W. D. S. Motherwell, F. H. Allen, *Acta Crystallogr. Sect. B* **2008**, *64*, 393–396; b) S. Lee, A. B. Mallik, D. C. Fredrickson, *Cryst. Growth Des.* **2004**, *4*, 279–290.

[25] G. R. Desiraju, T. Steiner, *The Weak Hydrogen Bond: In Structural Chemistry and Biology*, Oxford University Press, Oxford, **1999**, p. 507.

[26] S. D. Chakarova, E. Schröder, *J. Chem. Phys.* **2005**, *122*, 054102.

[27] a) M. Von Arnim, R. Ahlrichs, *J. Comput. Chem.* **1998**, *19*, 1746–1757; b) M. Häser and R. Ahlrichs, *J. Comput. Chem.* **1989**, *10*, 104–111; c) R. Ahlrichs, M. Bär, M. Häser, H. Horn, C. Kölmel, *Chem. Phys. Lett.* **1989**, *162*, 165–169.

[28] a) A. D. Becke, *J. Chem. Phys.* **1993**, *98*, 5648–5652; b) C. Lee, W. Yang, R. G. Parr, *Phys. Rev. B* **1988**, *37*, 785–789; c) A. D. Becke, *Phys. Rev. A* **1988**, *38*, 3098–3100.

[29] a) K. Eichkorn, F. Weigend, O. Treutler, R. Ahlrichs, *Theor. Chem. Acc.* **1997**, *97*, 119–124; b) M. Sierka, A. Hogekamp, R. Ahlrichs, *J. Chem. Phys.* **2003**, *118*, 9136–9148; c) K. Eichkorn, O. Treutler, H. Öhm, M. Häser, R. Ahlrichs, *Chem. Phys. Lett.* **1995**, *242*, 652–660.

[30] A. Schäfer, C. Huber, R. Ahlrichs, *J. Chem. Phys.* **1994**, *100*, 5829–5835.

[31] F. Pauly, J. K. Viljas, J. C. Cuevas, G. Schön, *Phys. Rev. B* **2008**, *77*, 155312.

[32] a) W. D. Xiao, Y. H. Jiang, K. Aït-Mansour, P. Ruffieux, H. J. Gao, R. Fasel, *J. Phys. Chem. C* **2010**, *114*, 6646–6649; b) C.-R. Lee, S. J. Bae, M.-S. Gong, K. Kim, S.-W. Joo, *J. Raman Spectrosc.* **2002**, *33*, 429–433.

[33] HOMO and LUMO levels of the dithiolcyclophane counterparts were calculated for comparison using similar DFT methods.

[34] a) A. Yassar, F. Demanze, A. Jaafari, M. El Idrissi, C. Coupry, *Adv. Funct. Mater.* **2002**, *12*, 699–708; b) N. R. Brinkmann, J. C. Rienstra-Kirakofe, H. F. Schaefer, *Mol. Phys.* **2001**, *99*, 663–675.

[35] U. Salzner, J. B. Lagowski, P. G. Pickup, R. A. Poirier, *J. Comput. Chem.* **1997**, *18*, 1943–1953.

[36] a) M. Tanaka, *Bull. Chem. Soc. Jpn.* **1976**, *49*, 3382–3388; b) T. Hoshi, H. Inoue, J. Shiraishi, Y. Tanizaki, *Bull. Chem. Soc. Jpn.* **1971**, *44*, 1743; c) M. Baiwir, M. Lomba, *Bull. Soc. R. Sci. Liege* **1972**, *41*, 531–536; d) H. H. Jaffé, M. Orchin, *Theory and Applications of Ultraviolet Spectroscopy*, Wiley, New York, **1963**, p. 624; e) D. Schweitzer, M. W. Haenel, *Chem. Ber.* **1985**, *118*, 163–175; f) H. Suzuki, *Bull. Chem. Soc. Jpn.* **1959**, *32*, 1357–1361; g) E. Clar, *Polycyclic Hydrocarbons, Vol. 2*, Academic Press, London and New York, **1964**, p. 6.

[37] J. Cornil, D. A. Dos Santos, D. Beljonne, J. L. Bredas, *J. Phys. Chem.* **1995**, *99*, 5604–5611.

[38] A. Tajiri, H. Uchimura, M. Hatano, *Chem. Lett.* **1975**, *4*, 1021–1024.

[39] H. Suzuki , *Electronic Absorption Spectra and Geometry of Organic Molecules: An Application of Molecular Orbital Theory*, Academic Press, New York, **1967**, p. 568.

[40] a) M. J. S. Dewar, *J. Am. Chem. Soc.* **1952**, *74*, 3345–3350; b) S. Woitellier, J. P. Launay, C. Joachim, *Chem. Phys.* **1989**, *131*, 481–488; c) A. C. Benniston, A. Harriman, *Chem. Soc. Rev.* **2006**, *35*, 169–179.

[41] a) A. Hargreaves, S. H. Rizvi, *Acta Crystallogr.* **1962**, *15*, 365–373; b) T. Yoshinaga, H. Hiratsuka, Y. Tanizaki, *Bull. Chem. Soc. Jpn.* **1978**, *51*, 996–1000; c) M. P. Johansson and J. Olsen, *J. Chem. Theory Comput.* **2008**, *4*, 1460–1471; d) O. Bastiansen, S. Samdal, *J. Mol. Struct.* **1985**, *128*, 115–125.

[42] J. Heinze, *Angew. Chem.* **1984**, *96*, 823–840; *Angew. Chem. Int. Ed. Engl.* **1984**, *23*, 831–847.
[43] a) P. H. Rieger, I. Bernal, W. H. Reinmuth, G. K. Fraenkel, *J. Am. Chem. Soc.* **1963**, *85*, 683–693; b) A. Baránski, W. R. Fawcett, *J. Electroanal. Chem.* **1979**, *100*, 185–196; c) W. R. Fawcett, J. S. Jaworski, *J. Phys. Chem.* **1983**, *87*, 2972–2976; d) A. Gennaro, A. M. Romanin, M. G. Severin and E. Vianello, *J. Electroanal. Chem.* **1984**, *169*, 279–285; e) A. Gennaro, F. Maran, A. Maye, E. Vianello, *J. Electroanal. Chem.* **1985**, *185*, 353–363; f) M. Sertel, A. Yildiz, H. Baumgärtel, *Electrochim. Acta* **1986**, *31*, 1625–1632; g) M. Sertel, A. Yildiz, R. Gambert, H. Baumgärtel, *Electrochim. Acta* **1986**, *31*, 1287–1292; h) A. Yildiz, M. Sertel, R. Gambert, H. Baumgärtel, *Electrochim. Acta* **1988**, *33*, 169–170.
[44] A. Nitzan, *J. Phys. Chem. A* **2001**, *105*, 2677–2679.
[45] a) P. Čársky, R. Zahradník, *Top. Curr. Chem.* **1973**, *43*, 1–55; b) S. F. Nelsen, M. N. Weaver, J. I. Zink, J. P. Telo, *J. Am. Chem. Soc.* **2005**, *127*, 10611–10622.

Received: December 31, 2010
Published online: May 12, 2011

